43.0   THERMODYNAMICS OF REFRACTORY ALLOYS

Robert Puerling (Mines)
Faculty: Amy Clarke (Mines), Jonah Klemm-Toole (Mines)
Industrial Mentors: Andy Deal (KCNSC), Wes Everhart (KCNSC), Noah Philips (ATI), Andrew Kustas (SNL)

This project initiated in Spring 2020 and is supported by the Kansas City National Security Campus (KCNSC). The research performed during this project will serve as the basis for a Master's thesis program for Robert Puerling.

43.1   Project Overview and Industrial Relevance

This project aims to assist in the development of refractory multi-principal element alloys (RMPEAs) by improving the predictive capabilities of Thermo-Calc with regards to refractory alloys in general. This will be achieved by investigations into the thermodynamics of MoNbTa, as it is currently not critically assessed within Thermo-Calc's high entropy alloy (HEA) database (TCHEA5). Due to lengthy heat treatment times at high temperatures, diffusion couples are being made to achieve a composition gradient throughout a single sample in a high throughput manner. The selection of MoNbTa was guided by literature review and solidification and diffusion simulations with Thermo-Calc's Scheil and DICTRA modules using the TCHEA4 and the HEA mobility (MOBHEA2) databases. The DICTRA and Scheil modules are also being used to guide the development of heat treatments. Once samples have been heat treated, their microstructures and phase stabilities will be characterized and assessed. The resulting data may inform additional Thermo-Calc simulations, perhaps comparing new predictions to the experimental data.

43.2   Previous Work

Multiple RMPEAs have been reported that show both promising high temperature strength and room temperature ductility [43.1-43.6]. MoNbTa is the most common ternary found within the seven alloys listed in Table 43.1, along with their mechanical properties, and is not considered to be critically assessed by Thermo-Calc. While assessing Thermo-Calc's DICTRA and Scheil modules' capabilities and using them to develop a heat treatment plan, an apparent issue with the diffusivity of Ta within the MOBHEA2 database was discovered. DICTRA predicts the Ta containing alloys MoNbTaTi and NbTaTiW homogenize faster than what is experimentally observed (Figures 43.1 and 43.2 and Tables 43.2 and 43.3). Micrographs (Figure 43.3) of the alloys show a length scale (proportional to the secondary dendrite arm spacing) of approximately of 20-30 μm, highlighting that segregation is still present after heat treatment. Yet, simulations show almost full homogenization to occur when the length scale is 10 μm for the NbTaTiW alloy, and for each of the length scales simulated for the MoNbTaTi alloy. Diffusion couples containing Ta diffuse more rapidly than what is calculated using interdiffusivity values [43.8], per equation 43.1:

$$L_D = \sqrt{D_o e^{\left(\frac{-E}{RT}\right)} t} \qquad [43.1]$$

where L_D is the diffusion length, D_o is the diffusion coefficient, E is the activation energy for diffusion, R is the ideal gas constant, and T is temperature. The results of these calculations (Table 43.4) do not agree with the simulations. According to the calculations, a diffusion couple of Ta and W should result in a diffusion length, measured from 50/50 Ta/W composition to 75/25 or 25/75, of about 13 μm, but the simulation (Figure 43.4) predicts a diffusion length of about 85 and 24 μm, respectively.

This led to diffusion couple simulations of Mo with Nb being used to guide the development of a heat treatment plan, as Mo and Ta have similar self-diffusivity values [43.9]. This heat treatment plan calls for heat treatments at three different temperatures for different times. First, to achieve a sufficient amount of diffusion through the diffusion couple (at least 100 μm), all samples would be heat treated at 2000˚C for 100 hours in vacuum. This initial heat

treatment would be followed by an additional 100 hours at 2000˚C for one-third of the samples, 400 hours at 1700˚C for another third of the samples, and 1000 hours at 1400˚C for the last third of the samples. However, an available vacuum furnace capable of the 2000˚C heat treatments could not be found. This led to investigating alternative heat treatment methods, including utilizing the vacuum hot press at the Colorado School of Mines (Mines) and an open-air box furnace. The hot press needed repairs to both the hot zone and the vacuum system to perform heat treatments above 1600˚C, while heat treatments in an open-air furnace require a nesting doll diffusion chamber, Figure 43.5, to prevent oxidation of the samples.

Diffusion couples were created using the Gleeble at Mines, where 5 mm cubes of Ta, coupled with Mo and MoNb binaries, and Mo coupled with a NbTa binary, were placed under compression, Figure 43.6. Once placed in the Gleeble under vacuum, the samples were heated to 1200˚C and held there for 30 min. Prior to being placed in the Gleeble, the faces of the cubes being joined were ground with 1200 grit SiC grinding media.

After repairs on the vacuum system of the hot press at Mines were completed and two trial heat treatments were performed, one sample set of diffusion couples (Mo-Ta, Mo-Nb7.5Ta, Ta-Mo10Nb, Ta-Mo30Nb, Ta-Nb50Mo, Ta-Nb30Mo, Ta-Nb10Mo) were heat treated at 1700˚C for a total of 420 hours in an Ar atmosphere with the hot press. Initial investigations showed about 35 μm of diffusion in the Mo-Ta diffusion couple (Figure 43.7). Back-Scatter Electron (BSE) images of each diffusion couple, Figure 43.8, show some contrast on the Ta side of the diffusion couple interfaces, as well as along most outside edges of the Ta in each diffusion couple. Energy Dispersive Spectroscopy (EDS) shows only Ta to be present (Figure 43.9). This suggests the contrast is due to channeling contrast, something deposited on the surface during polishing that EDS is penetrating through, or there are lighter elements present that EDS has trouble picking up, such as carbon or oxygen. Further investigation needed to be performed to determine the cause of this contrast.

One trial was performed to test the nesting doll diffusion chamber technique. For this first trial, a diffusion chamber (Figure 43.5) was built in an Ar glove box, with a Mo-Ta diffusion couple placed in the center. The diffusion chamber was heat treated in air (Ar was not hooked up to the furnace at the time) at 1500˚C for 24 hours. When disassembling the diffusion chamber, the Zr powder was found to have sintered into a solid. While the diffusion couple seemed to be intact with no oxidation, the Ta foil packet surrounding it was gone, suggesting there was enough oxygen present in the inner chamber to turn both layers of Ta foil into oxide. A comparison of the first hot press trial (Figure 43.10) and this trial (Figure 43.11) showed this nesting doll diffusion chamber technique to have promise. However, additional trial(s) needed to be performed.

43.3   Recent Progress

43.3.1   Additional Diffusion Couple Creation

Three more sample sets of diffusion couples were created, with slightly different methods for each sample set planned. The first had the joining faces of the samples ground with 1200 grit SiC grinding media, whereas the second and third were ground with 1200 grit Al_2O_3 grinding media. It was planned to have the first and second sample sets compressed 1 mm during the 30 min hold in the Gleeble, whereas the third sample set would not be compressed. However, due to issues welding the thermocouples to the samples, each sample was heated to ~900˚C in the Gleeble with no hold.

43.3.2   Additional Hot Press Heat Treatments and Results

The three sample sets of diffusion couples were heat treated in the hot press at 1700˚C for 500 hours in 100-hour segments in a static UHP Ar environment. Witness samples of Nb30Mo and Nb7.5Ta were also heat treated, with one of each pulled out at the end of each 100-hour segment. The Nb7.5Ta witness samples appeared to be eroding away more and more with each successive heat treatment. BSE images show three levels of contrast: a light matrix, medium contrast along the edges and throughout the samples, and the darkest contrast throughout the samples (Figure 43.12).

The images in Figure 43.12 were taken at the corner of the samples, which were initially sharp, showing the erosion. EDS spot scans, using an accelerating voltage of 5 keV to better pick up interstitials, show the matrix is Nb7.5Ta with C and O present; the medium contrast is a carbide and the darkest contrast is an oxide (Figure 43.13). BSE images of the Nb30Mo witness samples also show contrast throughout the samples (Figure 43.14). EDS spot scans show the matrix to be Mo30Nb with high levels of C, the medium contrast is a niobium carbide with some N present and little to no Mo, and the darkest contrast is a niobium oxide with little to no Mo present (Figure 43.15).

Initial investigations into the diffusion couples showed there to be no difference between the sample set ground with SiC and those ground with AlO. One of the sample sets ground with AlO was sent to KCNSC for chemical analysis. The contrast observed on the Ta side of the interface of the samples previously heat treated for 420 hours at 1700˚C appears in each of the Ta-Nb50Mo, Ta-Nb30Mo, and Ta-Nb10Mo heat treated samples (Figure 43.16), but is absent in the Mo-Ta, Ta-Mo10Nb, Ta-Mo30Nb, and Mo-Nb7.5Ta samples (Figure 43.17). EDS line scans of this area, using an accelerating voltage of 5keV to better pick up interstitials, show the darker areas to be high in C (Figure 43.18). Due to Ta and Nb's high affinity for C and Mo's low affinity for C (Figure 43.19), it is hypothesized the contrast at the interface of the diffusion couples of Ta with the higher Nb content binaries is due to C diffusing quickly into the Nb binary, then being leeched by the Ta, creating a tantalum carbide at the interface. Further from the interface, additional contrast is observed along the grain boundaries of the Ta in each diffusion couple (Figures 43.16 and 43.17). EDS shows these areas to be oxide (Figure 43.20). Contrast is also observed throughout the Nb7.5Ta, Nb30Mo, and Nb10Mo, as was observed in the witness samples of Nb7.5Ta and Nb30Mo.

It is unknown what the denuded zone observed in the Mo-Ta, Ta-Mo10Nb, Ta-Mo30Nb, Mo-Nb7.5Ta is caused by. It is not the initial interface of the diffusion couple, as a scratch was placed on the Ta side of one of the Mo10Nb diffusion couples to track the initial interface (Figure 43.20(d)). Electron Backscatter Diffraction (EBSD) also shows this zone is not attributed to recrystallization (Figure 43.21). Further investigation needs to be done to determine the cause of this denuded zone.

The high C content in the heat-treated samples is likely due to heat treating in a static atmosphere with an entirely graphite hot zone. An additional heat treatment was performed on one Nb7.5Ta sample and one Nb30Mo sample. In this heat treatment the setup was the same as the previous heat treatment in the hot press with a change to the environment: flowing, instead of static, UHP Ar. Due to an issue with the hot press, the run stopped short of the 100-hour goal, only reaching 68 hours at 1700 ˚C. The Nb7.5Ta sample did not erode like the witness samples from the previous heat treatment, but BSE images still show contrast in both the Nb7.5Ta and Nb30Mo samples (Figure 43.22). EDS line scans show the darker contrast areas in both samples to be high in N (Figures 43.24 and 43.25). Although there was N contamination, the flowing Ar environment appears to be better than the static one, as there was significantly less O and C contamination.

43.3.3 Second Diffusion Chamber Heat Treatment Trial

A second trial of the nesting doll diffusion chamber was performed at 1500 ˚C for 72 hours with flowing UHP Ar. This nesting doll diffusion chamber was built the same way as the first trial, in an Ar glove box. Although the first trial showed promise, the second trial was a failure (Figure 43.25). This failure led to investigations into this method of heat treatment to be postponed indefinitely, in favor of focusing on the hot press heat treatments.

43.4 Plans for Next Reporting Period

- Complete microstructural characterization and phase stability assessment.
- Input experimental data into Thermo-Calc and compare new predictions to experimental data.
- Write and defend thesis.

43.5   References (See external document on references)

[43.1] O.N. Senkov, D.B. Miracle and K.J. Chaput, "Development and exploration of refractory high entropy alloys—A Review," Journal of Materials Research, vol. 33, no. 19, pp. 3092-3128, 2018.

[43.2] O.A. Waseem, J. Lee, H.M. Lee, and H.J. Ryu, "The effect of Ti on the sintering and mechanical properties of refractory high-entropy alloy TixWTaVCr fabricated via spark plasma sintering for fusion plasma-facing materials," Materials Chemistry and Physics, vol. 210, pp. 87–94, 2018.

[43.3] C.C. Juan et al., "Enhanced mechanical properties of HfMoTaTiZr and HfMoNbTaTiZr refractory high-entropy alloys," Intermetallics, vol. 62, pp. 76–83, 2015.

[43.4] O. Senkov, G. Wilks, J. Scott, and D. Miracle, "Mechanical properties of Nb25Mo25Ta25W25 and V20Nb20Mo20Ta20W20 refractory high entropy alloys," Intermetallics, vol. 19, no. 5, pp. 698–706, 2011.

[43.5] Z. Han et al., "Effect of Ti additions on mechanical properties of NbMoTaW and VNbMoTaW refractory high entropy alloys," Intermetallics, vol. 84, pp. 153–157, 2017.

[43.6] F.G. Coury, M. Kaufman, and A.J. Clarke, "Solid-solution strengthening in refractory high entropy alloys," Acta Materialia, vol. 175, pp. 66–81, 2019.

[43.7] F.G. Coury et al., "Phase equilibria, mechanical properties and design of quaternary refractory high entropy alloys," *Materials & Design*, vol. 155, no. C, pp. 244–256, 2018.

[43.8] W. F. Gale and T. C. Totemeier, "Diffusion in Metals," in *Smithells Metals Reference Book*, 8th ed., 2004, pp. 73-100.

[43.9] H. Mehrer, N. Stolica and N. A. Stolwijk, "2.2 The self-diffusion tables," in *Diffusion in Solid Metals and Alloys*, Vols. Landolt-Bornstein - Group III Condensed Matter 26, 1990, pp. 34-66.

[43.10] S. R. Shatynski, "The Thermochemistry of Transition Metal Carbides," *Oxidation of Metals*, vol. 13, no. 2, pp. 105-118, 1979.

43.6 Figures and Tables

Table 43.1: RMPEAs with promising high temperature strength and room temperature fracture strain and their respective compression test data.

Alloy	RT Fracture Strain (%)	Yield Strength (MPa) @ 1000 ˚C	Yield Strength (MPa) @ 1200 ˚C	References
CrTaTiVW*	1.5	--	586	43.1, 43.2
HfMoNbTaTiZr	12	814	556	43.1, 43.3
MoNbTaW	2.6	548	506	43.1, 43.4, 43.5
MoNbTaVW	1.7	842	735	43.1, 43.4, 43.5
MoNbTaTiW	14.1	620	586	43.1, 43.5
MoNbTaTiVW	10.6	752.8	659	43.1, 43.5
CrMoTaTi	~13	~1150	--	43.6
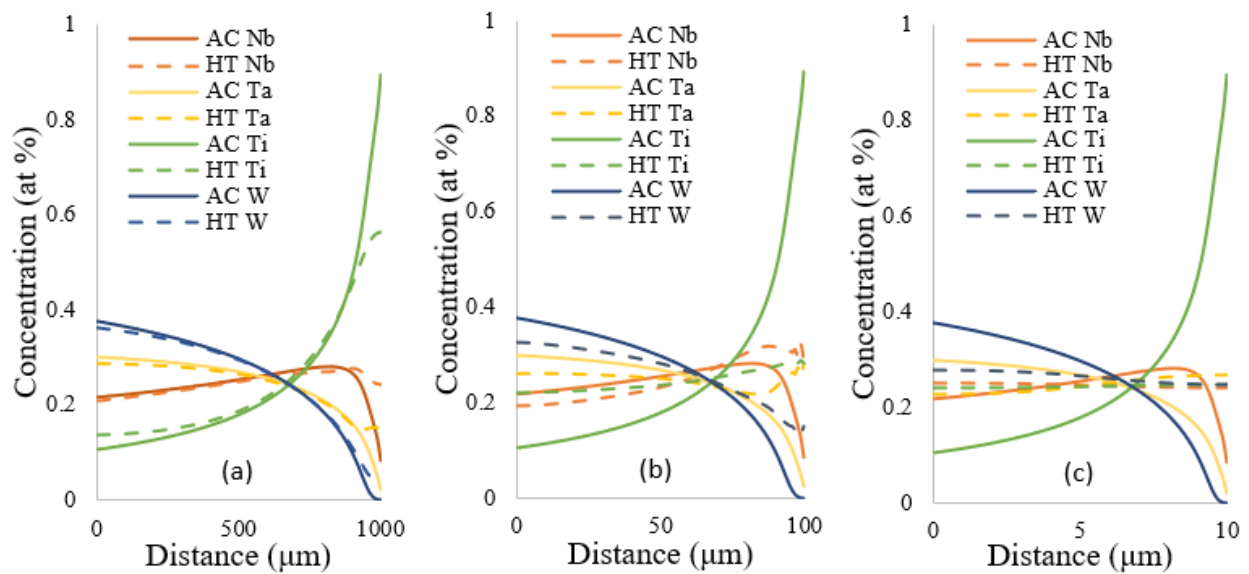
Figure 43.1: Solidification and homogenization simulations performed on NbTaTiW at length scales of (a) 1000 μm, (b) 100 μm, and (c) 10 μm, where AC is As-Cast, and HT is Heat-Treated.
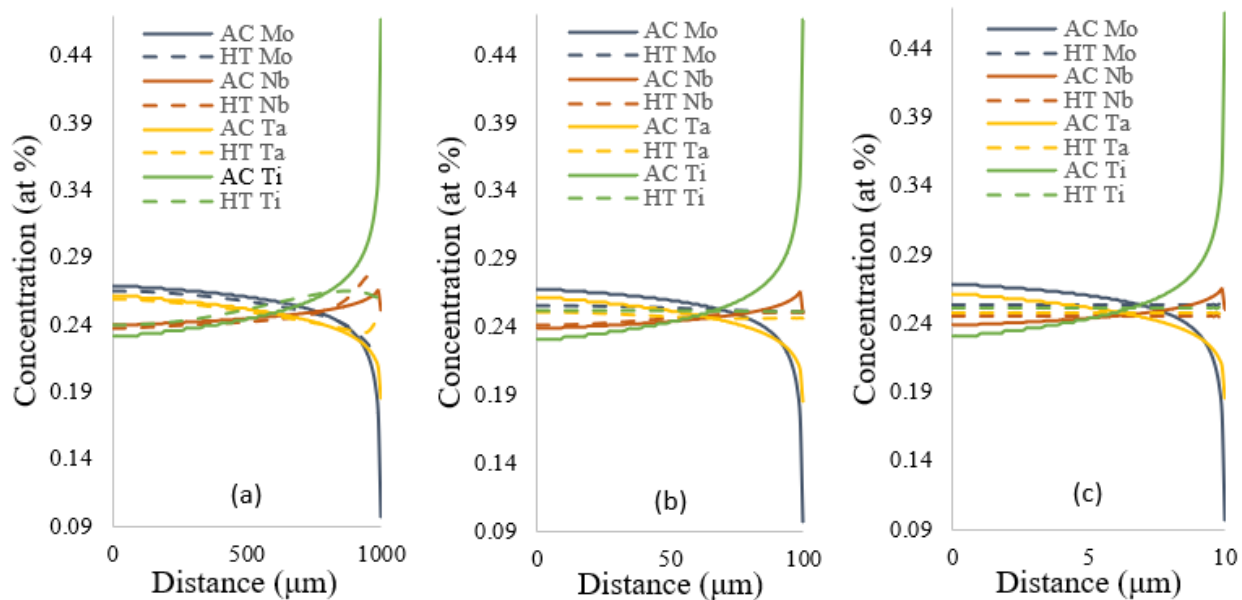
Figure 43.2: Solidification and homogenization simulations performed on MoNbTaTi at length scales of (a) 1000 μm, (b) 100 μm, and (c) 10 μm, where AC is As-Cast, and HT is Heat-Treated.

Table 43.2: Heat treated compositional (at%) data for NbTaTiW experiments [43.7] and simulations, where the average difference is the average of the absolute value difference between experimental and simulation data.

			Nb	Ta	Ti	W	Avg. Diff.
Dendrite Core	**Experimental**		23.2	27.9	19.8	29.1	--
	Simulated	**1000 μm**	24.1	27.4	16.7	31.6	1.75
		100 μm	22.1	25.3	23.2	29.4	1.85
		10 μm	24.9	23.8	24.2	27.1	3.05
Interdendritic	**Experimental**		26.5	23.9	26.3	23.5	--
	Simulated	**1000 μm**	26.6	23.1	27.1	23.2	0.5
		100 μm	27.8	23.0	25.4	23.9	0.875
		10 μm	24.2	25.8	24.5	25.5	2.0

Table 43.3: Heat treated compositional (at%) data for MoNbTaTi experiments [43.7] and simulations, where the average difference is the average of the absolute value difference between experimental and simulation data.

			Mo	Nb	Ta	Ti	Avg. Diff.
Dendrite Core	**Experimental**		21.7	22.3	33.5	21.4	--
	Simulated	**1000 μm**	26.5	23.7	25.9	23.9	4.075
		100 μm	25.5	24.1	25.1	25.2	4.125
		10 μm	25.4	24.6	24.8	25.2	4.625
Interdendritic	**Experimental**		22.8	24.5	25.5	28.4	--
	Simulated	**1000 μm**	21.7	27.8	24.5	26.0	1.95
		100 μm	25.2	25.0	24.7	25.2	1.725
		10 μm	25.4	24.6	24.8	25.2	1.925
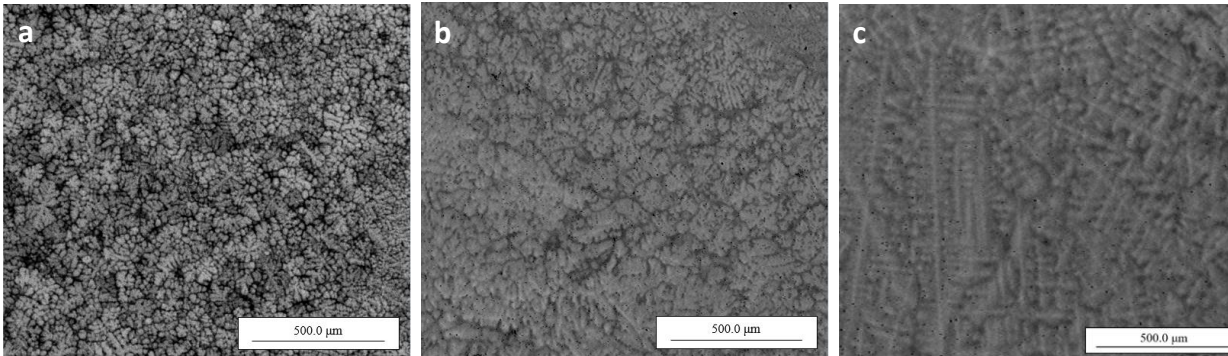
Figure 43.3: SEM BSE micrographs of (a) as-cast NbTaTiW, (b) heat treated (1400 ˚C for 35 h) NbTaTiW, and (c) heat treated (1400 ˚C for 35 h) MoNbTaTi.

Table 43.4: Diffusion calculations

	D_0 (10^{-4} m^{2}s^{-1})		E (kJ mol^{-1})		Temperature Window (K)		L_D (μm)
Ta in Ta$_{30}$W$_{70}$	1.8	[43.9]	553.9	[43.9]	1573-2373	[43.9]	12.6
W in Ta$_{30}$W$_{70}$	0.17	[43.9]	510.8	[43.9]	1573-2373	[43.9]	13.2
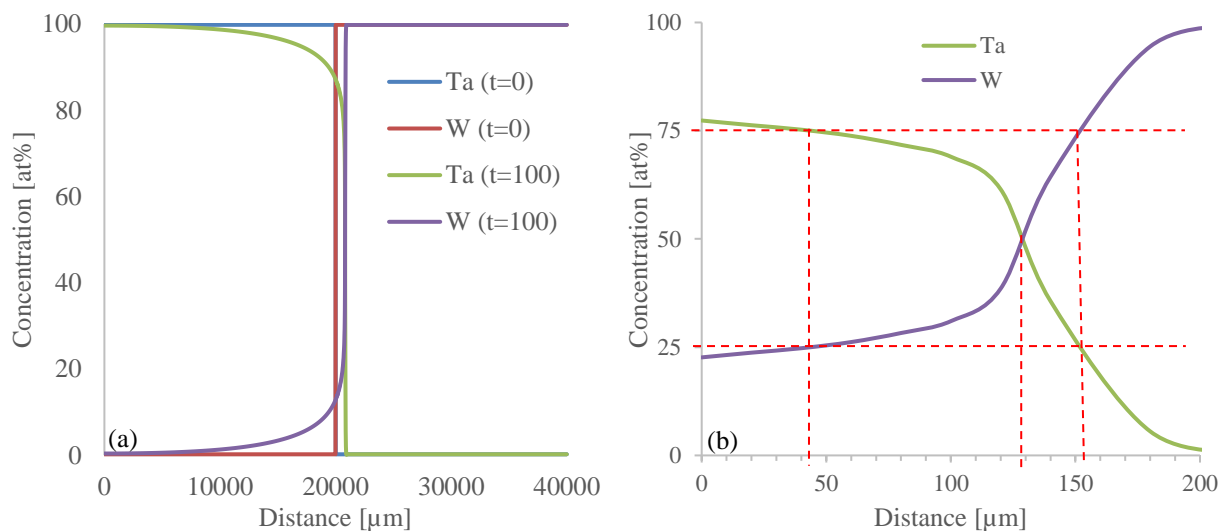
Figure 43.4: Diffusion couple simulation of Ta with W, using DICTRA, where the couple is heat treated at 1800 ˚C for 100 h. (a) The entire simulation data and (b) zoomed in around the interface after heat treatment, with lines indicating the locations of 75/25, 50/50, and 25/75 Ta/W.
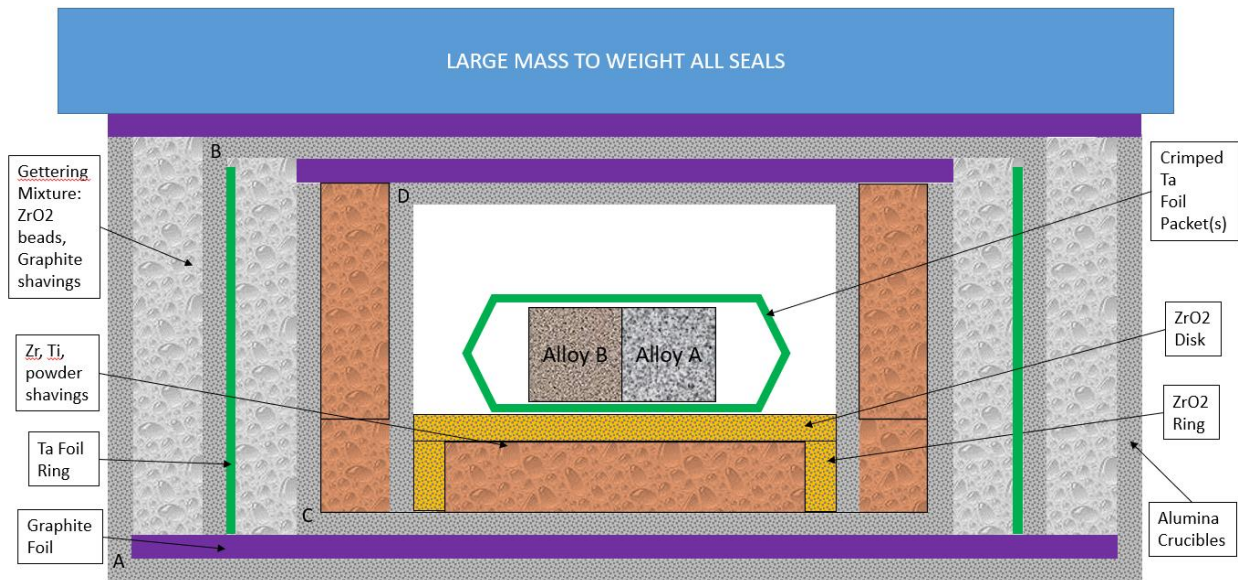
Figure 43.5: Diagram for nesting doll diffusion chamber.
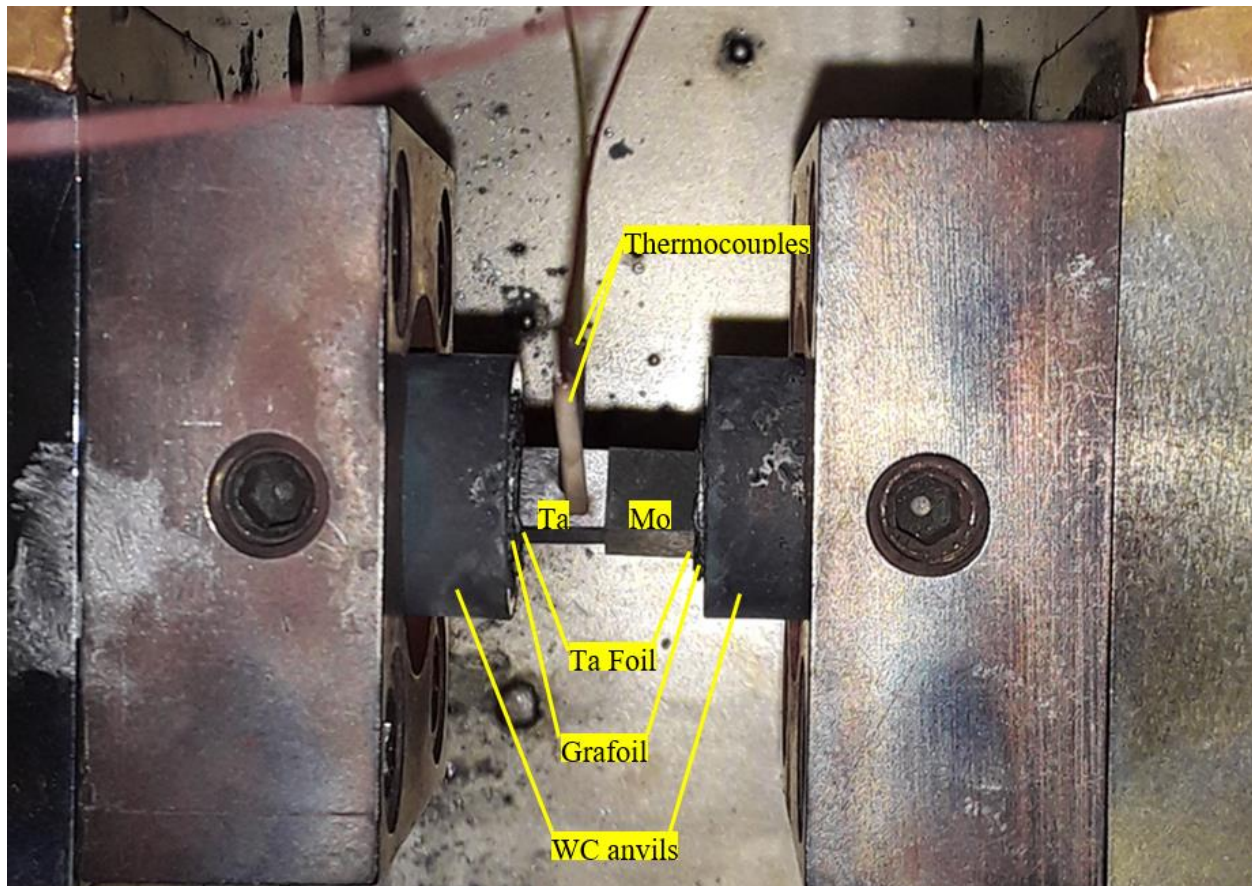
Figure 43.6: Diagram for diffusion couple creation in the Gleeble.
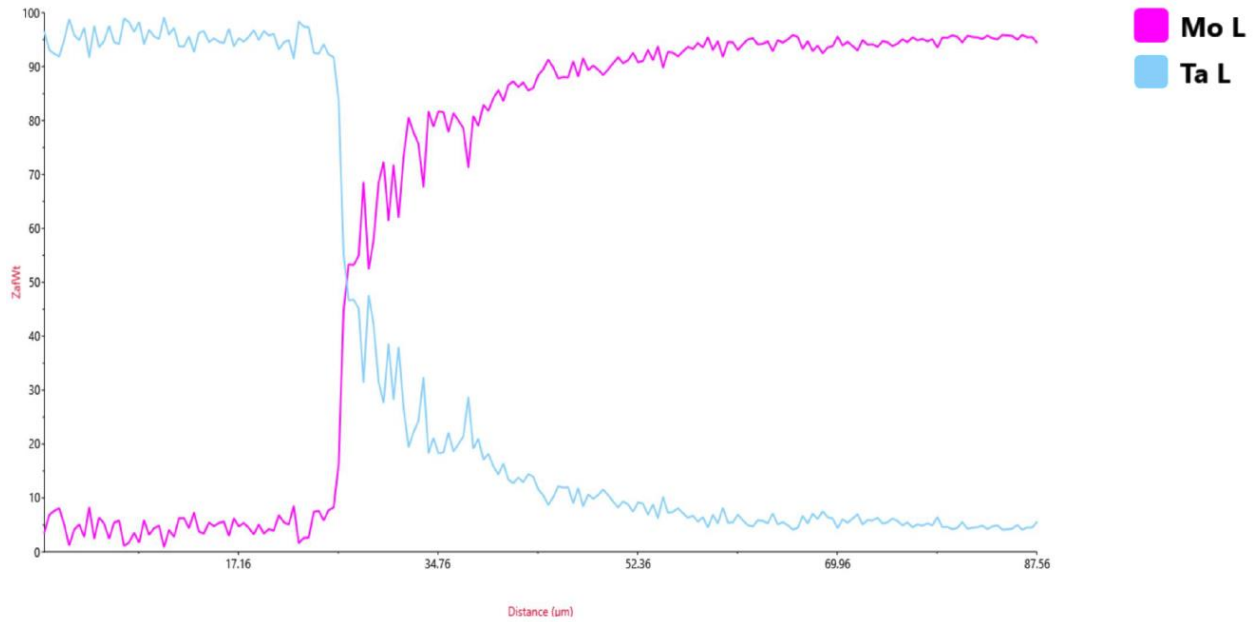
Figure 43.7: EDS line scan of the Mo-Ta diffusion couple, heat treated at 1700 ˚C for 420 h.
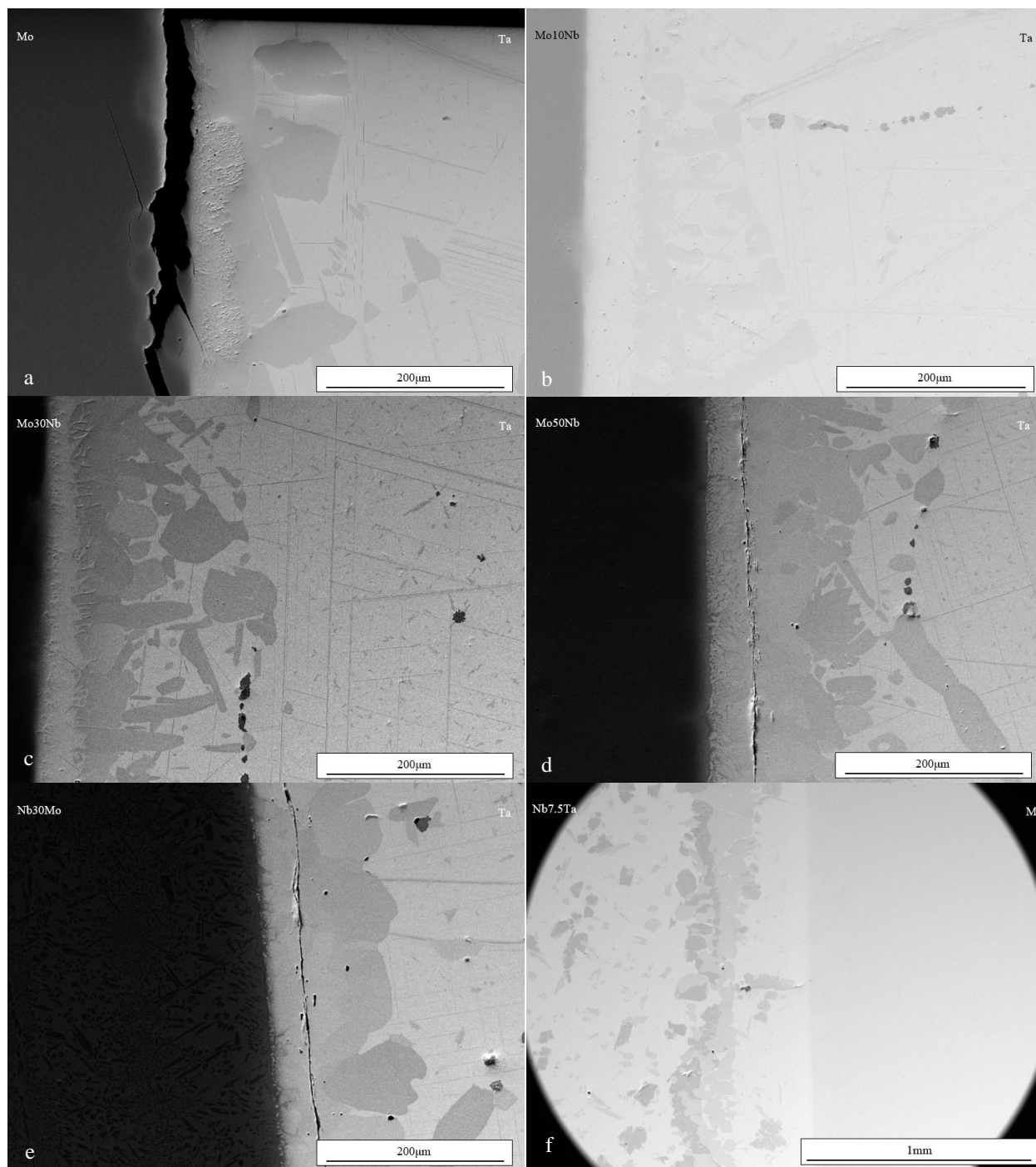
Figure 43.8: BSE images of the diffusion couples heat treated at 1700 ˚C for 420 h. The diffusion couples are (a) Mo-Ta, (b) Ta-Mo10Nb, (c) Ta-Mo30Nb, (d) Ta-Mo50Nb, (e) Ta-Nb30Mo, and (f) Mo-Nb7.5Ta.
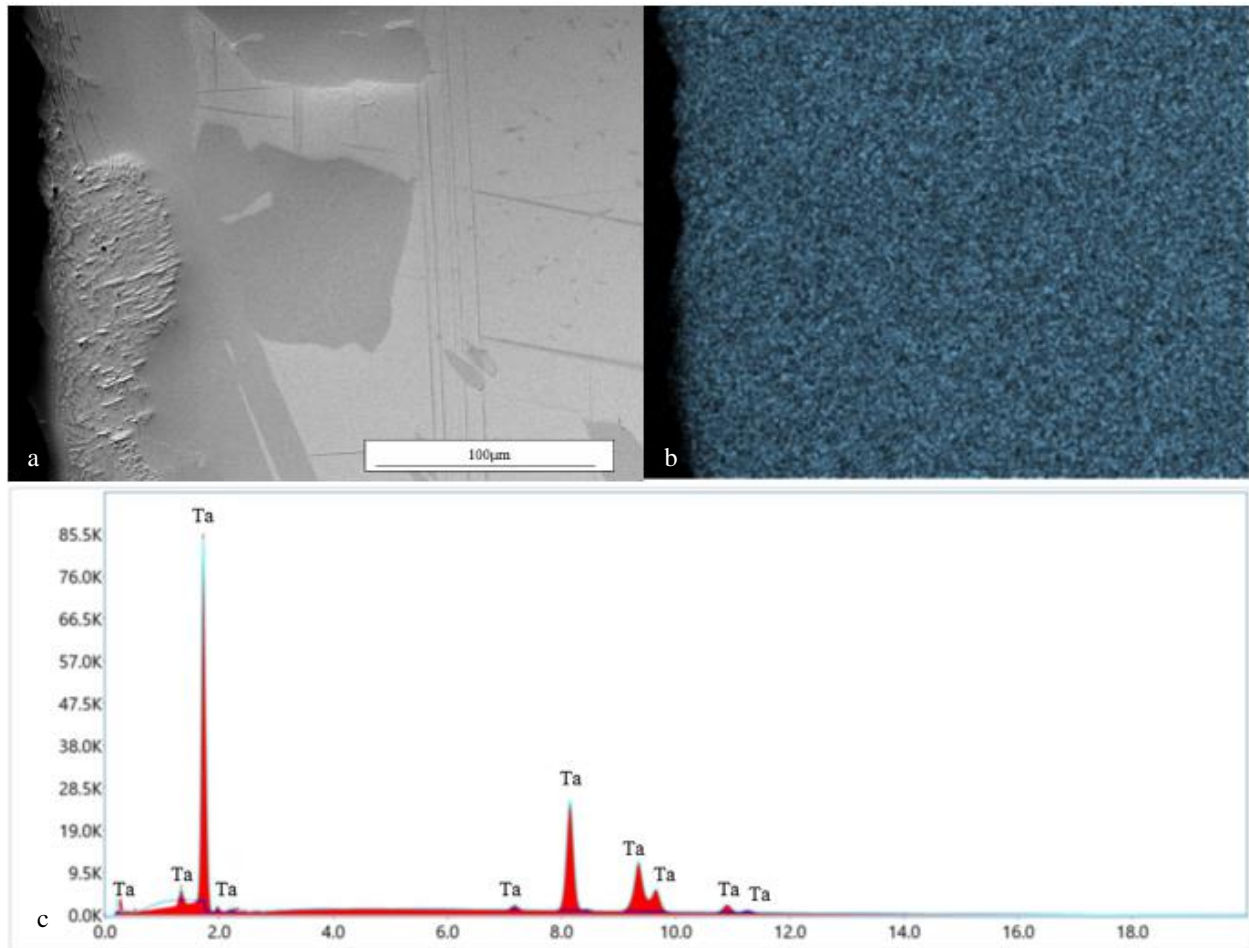
Figure 43.9: (a) BSE image of Ta side of the interface of the Mo-Ta diffusion couple heat treated at 1700°C for 420 h. (b) EDS map of the area seen in the BSE image, where the blue is Ta. (c) EDS spectrum analysis of the area seen in the BSE image, where each peak detected is accounted for by Ta.
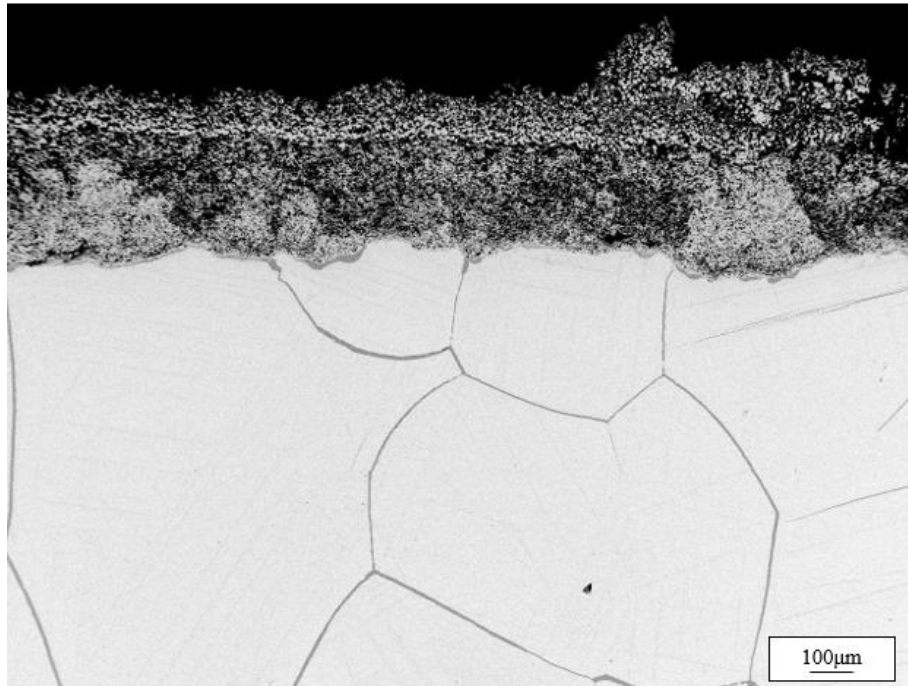
Figure 43.10: Secondary electron image of the edge of the Ta side of the Mo-Ta diffusion couple used for the first trial heat treatment in the hot press. Image was taken using the FESEM at Mines.
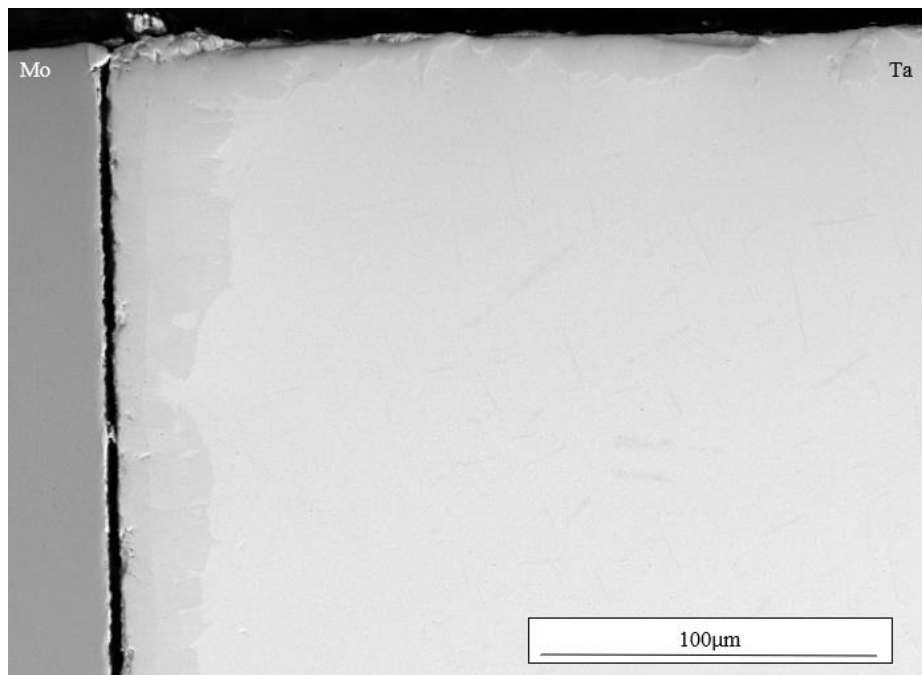
Figure 43.11: BSE image of the Mo-Ta diffusion couple heat treated during the nesting doll diffusion chamber trial. The crack at the interface was caused by cutting the diffusion couple in half, orthogonal to the interface, after heat treatment.
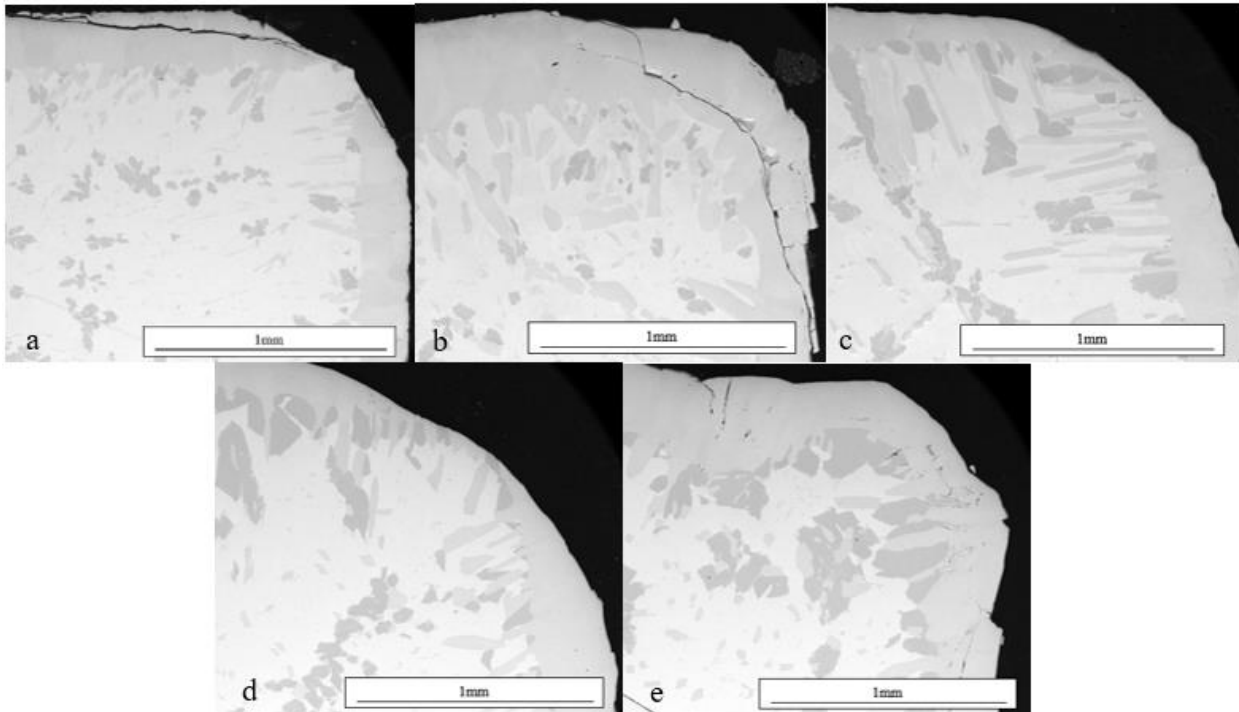
Figure 43.12: BSE images of Nb7.5Ta witness samples heat treated using the hot press at Mines in a static UHP Ar environment at 1700˚C for (a) 100h, (b) 200h, (c) 300h, (d) 400h, and (e) 500h.
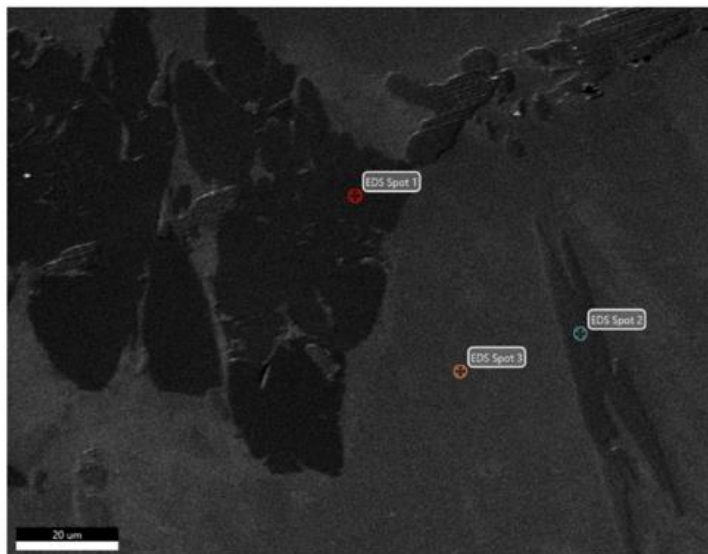
Smart Quant Results

Element	Weight %	Atomic %	Error %
Witness Samples | Nb7.5Ta 100hrs | Area 3 | EDS Spot 1			
C K	7.63	23.36	17.64
O K	21.52	49.48	10.84
NbL	66.18	26.21	10.03
TaM	4.68	0.95	19.43
Witness Samples | Nb7.5Ta 100hrs | Area 3 | EDS Spot 2			
C K	17.13	56.43	14.98
O K	4.53	11.2	17.5
NbL	73.62	31.34	9.76
TaM	4.72	1.03	21.84
Witness Samples | Nb7.5Ta 100hrs | Area 3 | EDS Spot 3			
C K	6.38	31.97	21.19
O K	3.08	11.61	19.03
NbL	83.4	54.05	9.68
TaM	7.14	2.38	13.77

Figure 43.13: EDS spot scans of the Nb7.5Ta witness sample heat treated using the hot press at Mines in a static UHP Ar environment at 1700 ˚C for 100 h. These spot scans are also representative of the Nb7.5Ta witness samples heat treated for 200, 300, 400, and 500 h.

7
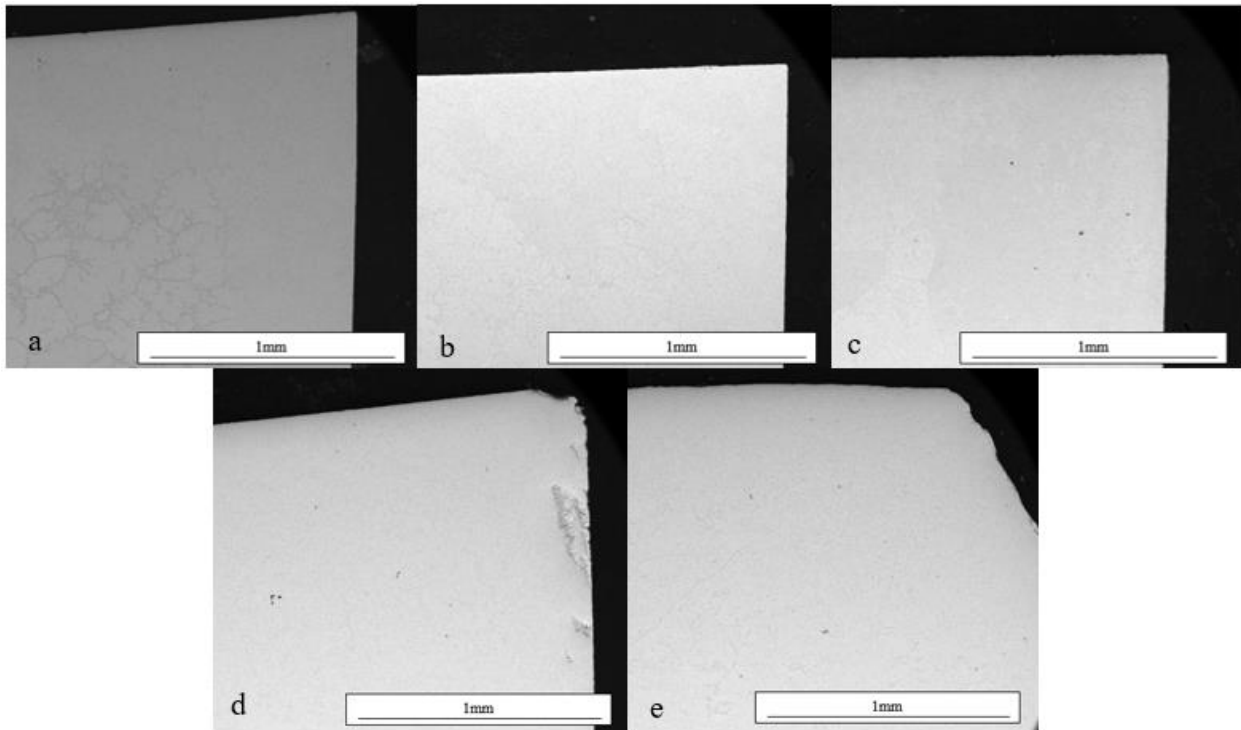
Figure 43.14: BSE images of Nb30Mo witness samples heat treated using the hot press at Mines in a static UHP Ar environment at 1700 ˚C for (a) 100 h, (b) 200 h, (c) 300 h, (d) 400 h, and (e) 500 h.
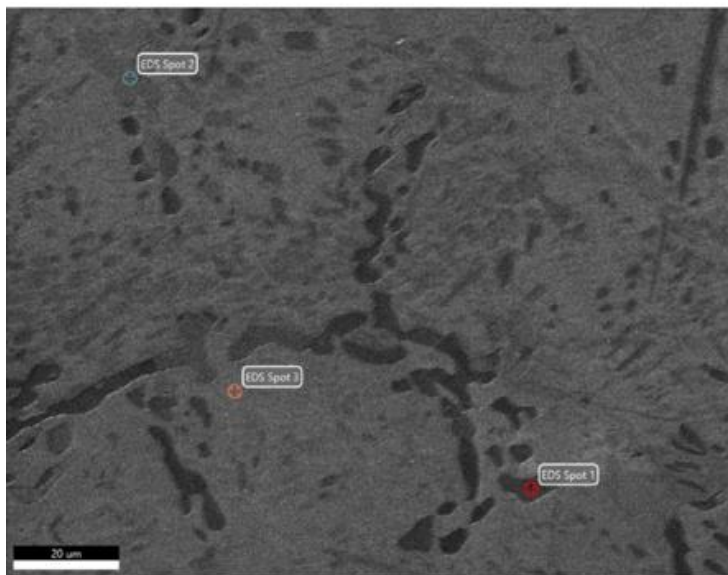
Smart Quant Results

Element	Weight %	Atomic %	Error %
Witness Samples | Nb30Mo 100hrs | Area 8 | EDS Spot 1			
C K	9.87	28.14	16.86
N K	0.47	1.14	89.72
O K	21.26	45.51	10.88
NbL	68.25	25.16	9.33
MoL	0.15	0.05	99.99
Witness Samples | Nb30Mo 100hrs | Area 8 | EDS Spot 2			
C K	20	58.37	13.78
N K	3.57	8.93	26.45
O K	2.13	4.68	25.75
NbL	73.25	27.64	9.2
MoL	1.05	0.38	87.29
Witness Samples | Nb30Mo 100hrs | Area 8 | EDS Spot 3			
C K	14.34	53.54	15.44
N K	0.01	0.02	99.99
O K	2.38	6.68	20.3
NbL	54.37	26.24	10.09
MoL	28.9	13.51	14.91

Figure 43.15: EDS spot scans of the Nb30Mo witness sample heat treated using the hot press at Mines in a static UHP Ar environment at 1700 ˚C for 100 h. These spot scans are also representative of the Nb30Mo witness samples heat treated for 200, 300, 400, and 500 h.
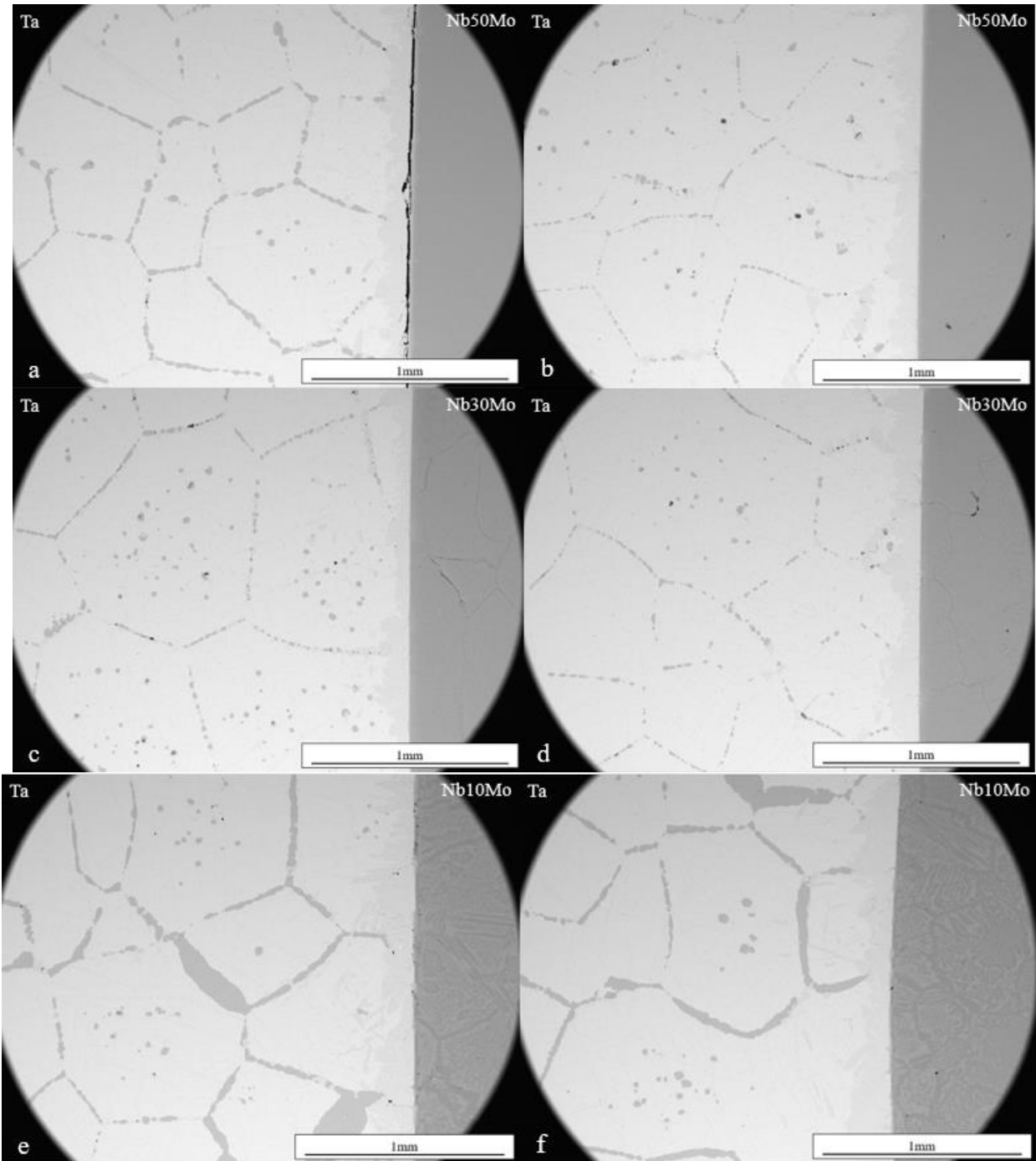
Figure 43.16: BSE images of (a)(b) Ta-Nb50Mo, (c)(d) Ta-Nb30Mo, and (e)(f) Ta-Nb10Mo diffusion couples heat treated using the hot press at Mines in a static UHP Ar environment at 1700 ˚C for 500 h, where samples (a)(c)(e) were ground with SiC media and samples (b)(d)(f) were ground with AlO media prior to diffusion couple creation. The rounded edge of each image is the edge of the imaging lens.
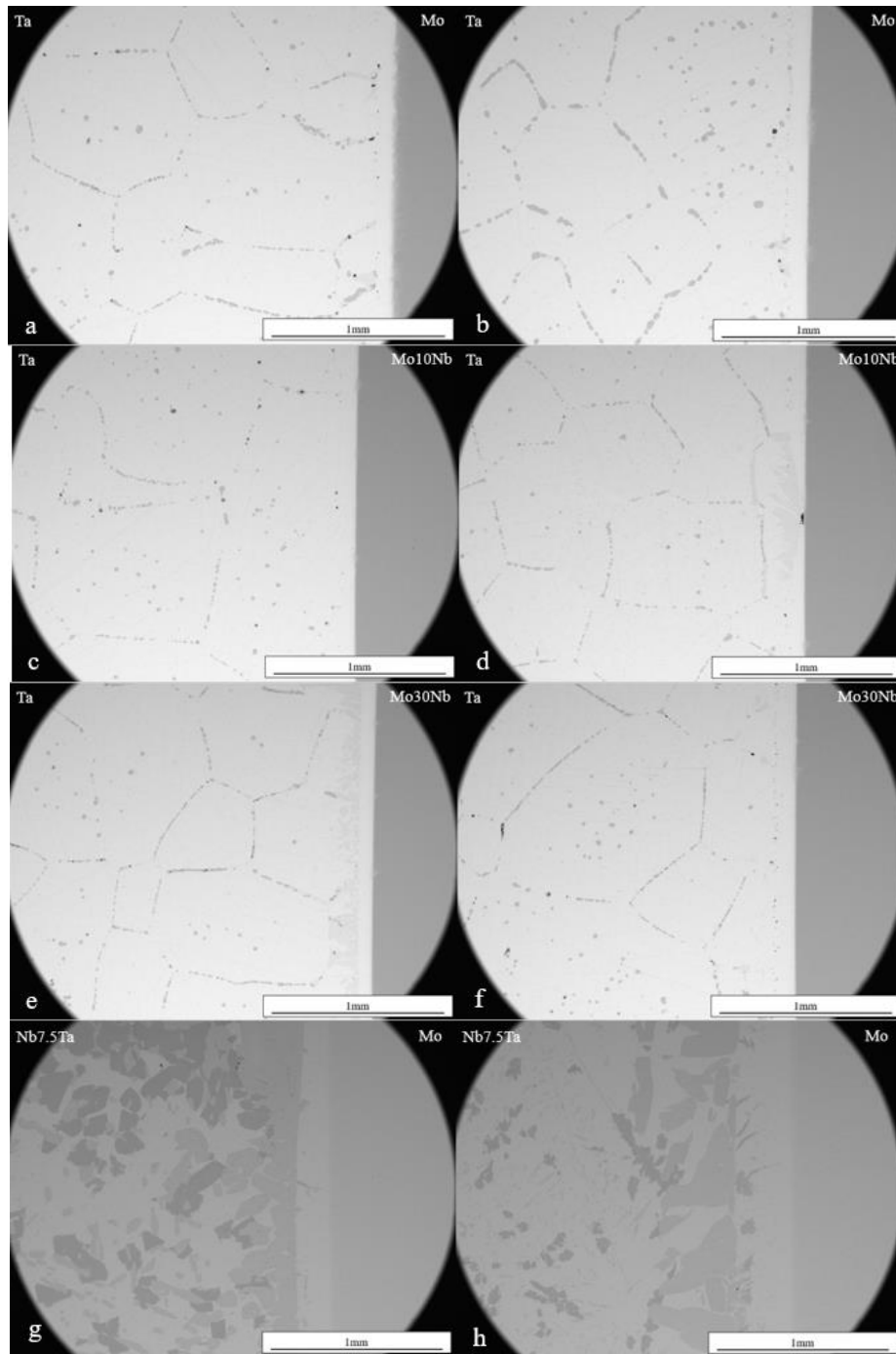
Figure 43.17: BSE images of (a)(b) Mo-Ta, (c)(d) Ta-Mo10Nb, (e)(f) Ta-Mo30Nb, and (g)(h) Mo-Nb7.5Ta
diffusion couples heat treated using the hot press at Mines in a static UHP Ar environment at 1700 ˚C
for 500 h, where samples (a)(c)(e)(g) were ground with SiC media and samples (b)(d)(f)(h) were
ground with AlO media prior to diffusion couple creation. The rounded edge of each image is the edge
of the imaging lens.
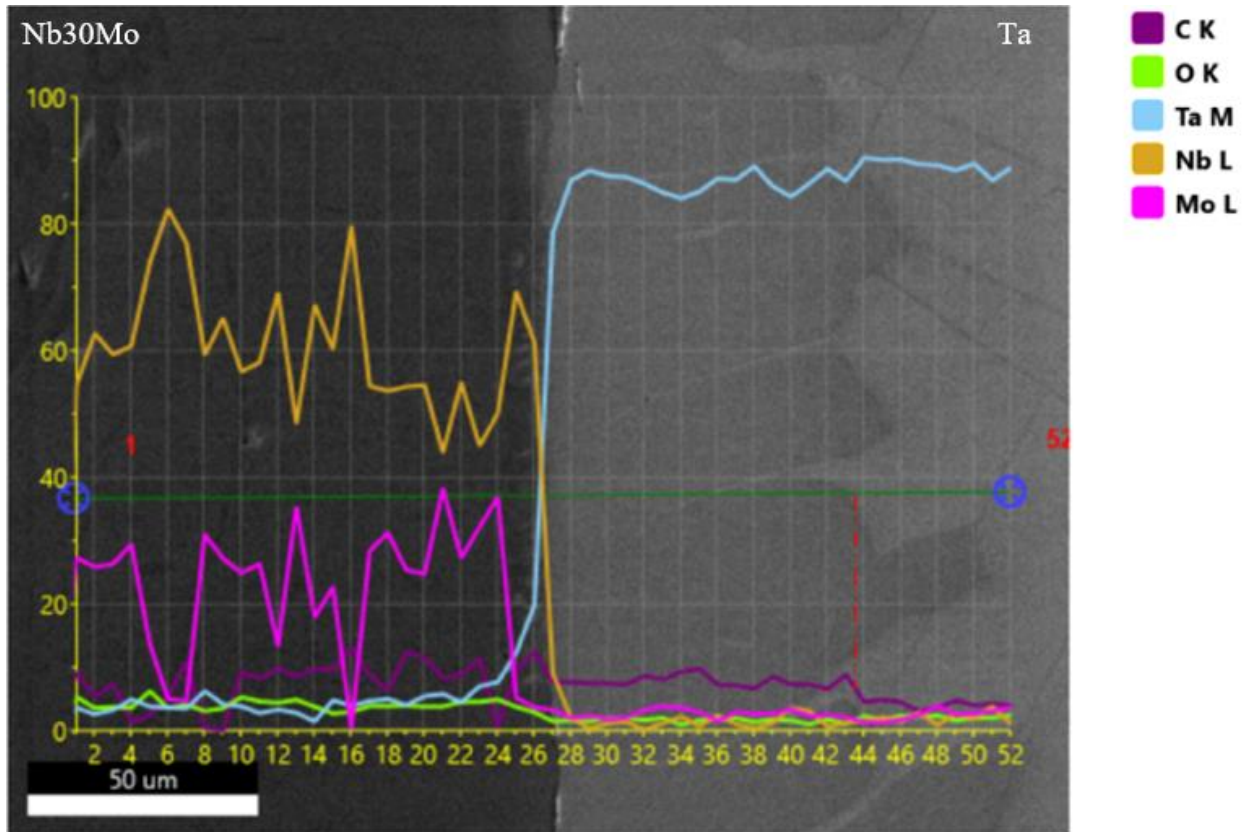
Figure 43.18: EDS line scan of the Ta-Nb30Mo diffusion couple heat treated using the hot press at Mines in a static UHP Ar environment at 1700 ˚C for 500 h, where the green line indicates where the line scan was performed.
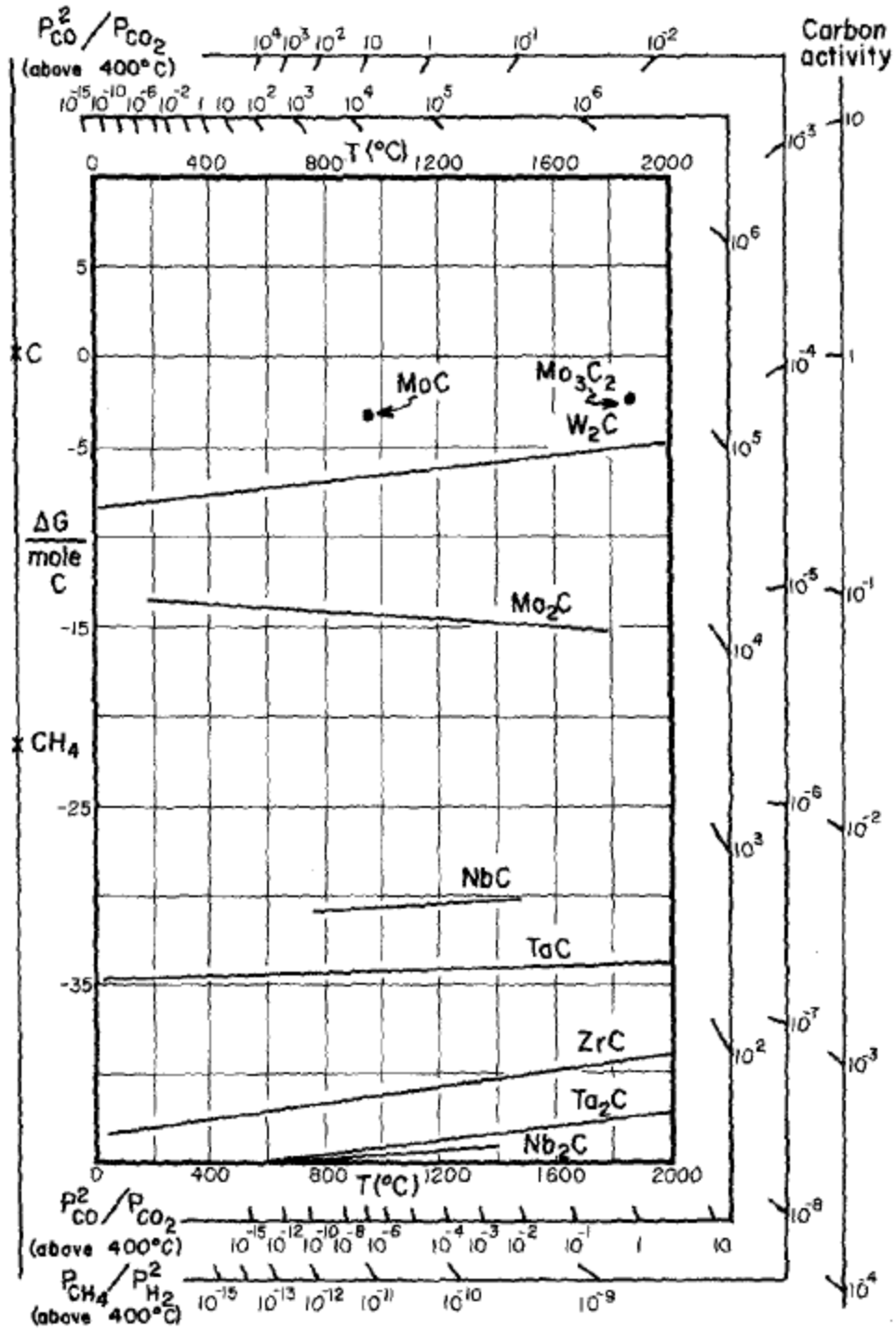
Figure 43.19: Ellingham diagram for the second and third transition series carbides. [43.10]
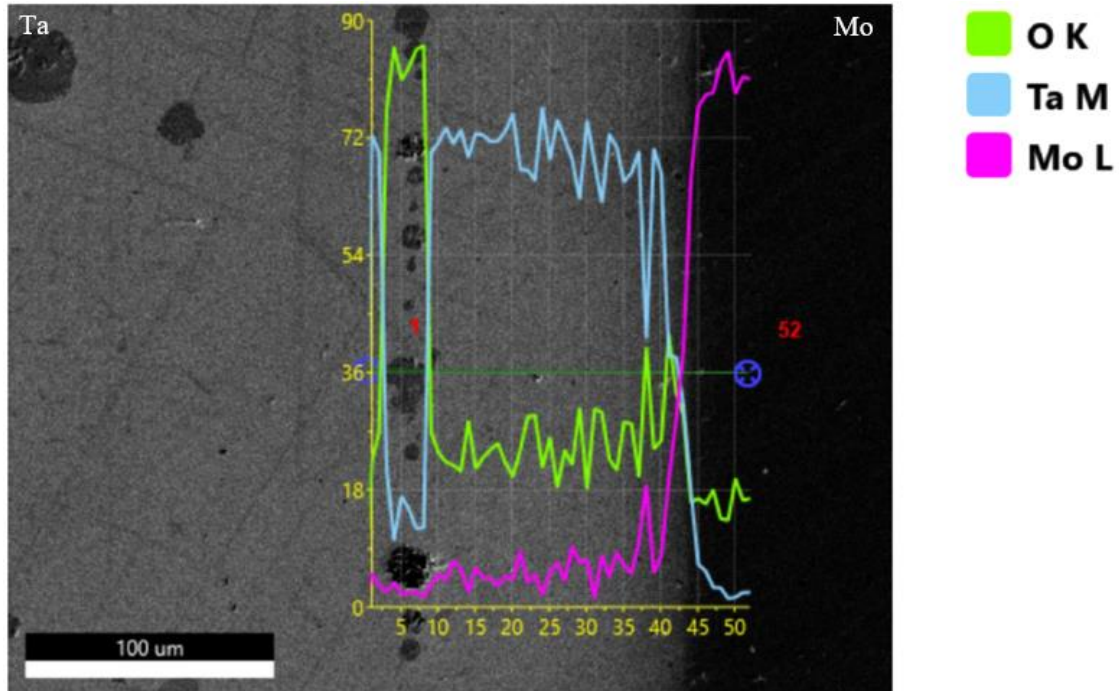
Figure 43.20: EDS line scan of the Mo-Ta diffusion couple heat treated using the hot press at Mines in a static UHP Ar environment at 1700 °C for 500 h, where the dark green line indicates where the line scan was performed.
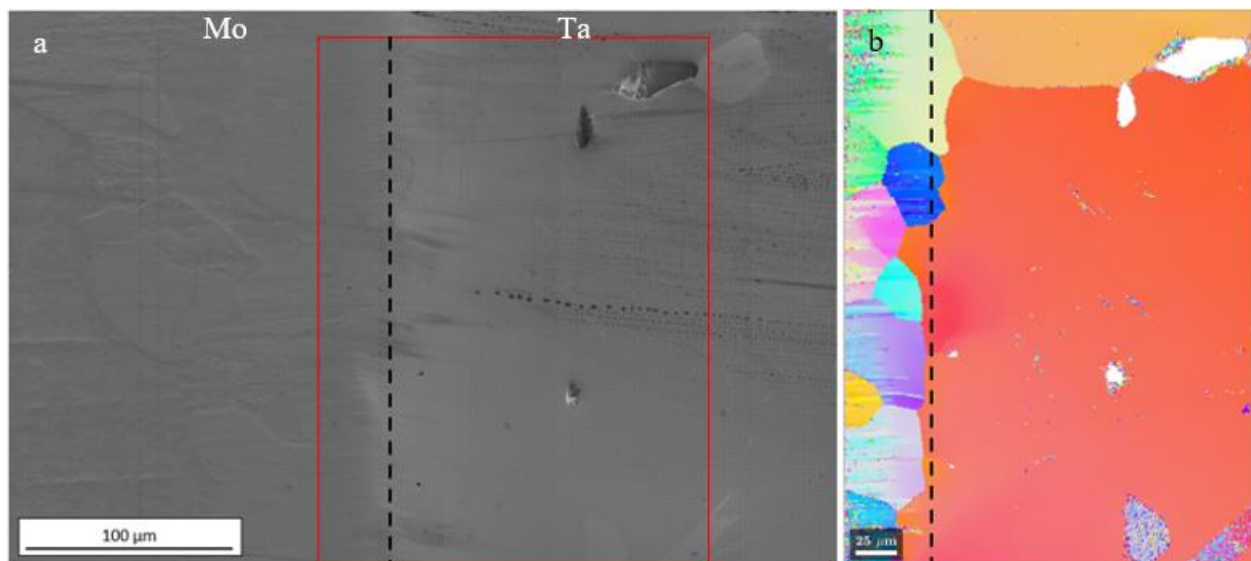
Figure 43.21: (a) SE image of the Mo-Ta diffusion couple heat treated using the hot press at Mines in a static UHP Ar environment at 1700 °C for 500 h, where the red box indicates the area over which an EBSD scan (b) was performed. The black dashed indicate the interface of the diffusion couple.
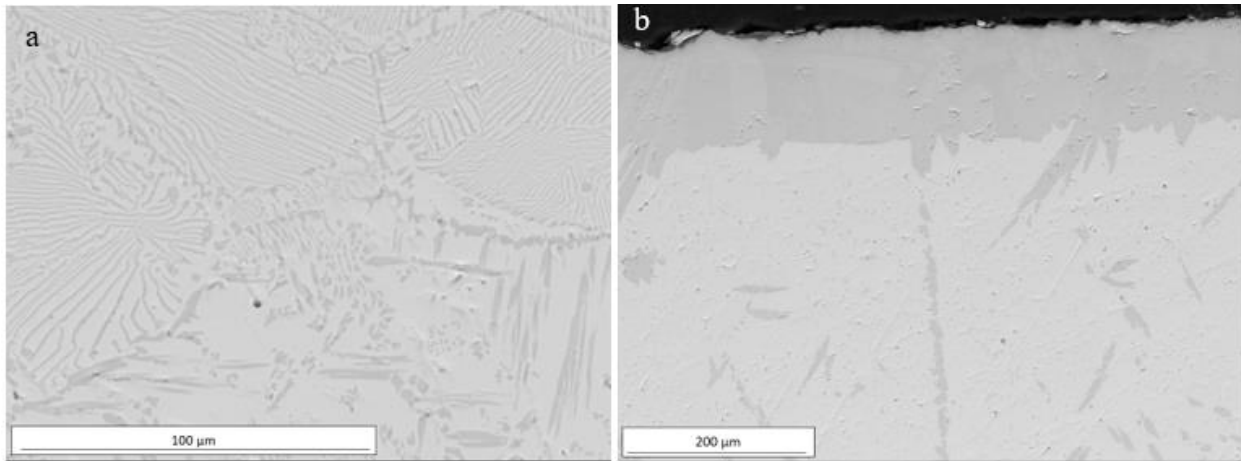
Figure 43.22: BSE images of (a) Nb30Mo and (b) Nb7.5Ta heat treated using the hot press at Mines in a flowing UHP Ar environment at 1700 ˚C for 68 h.
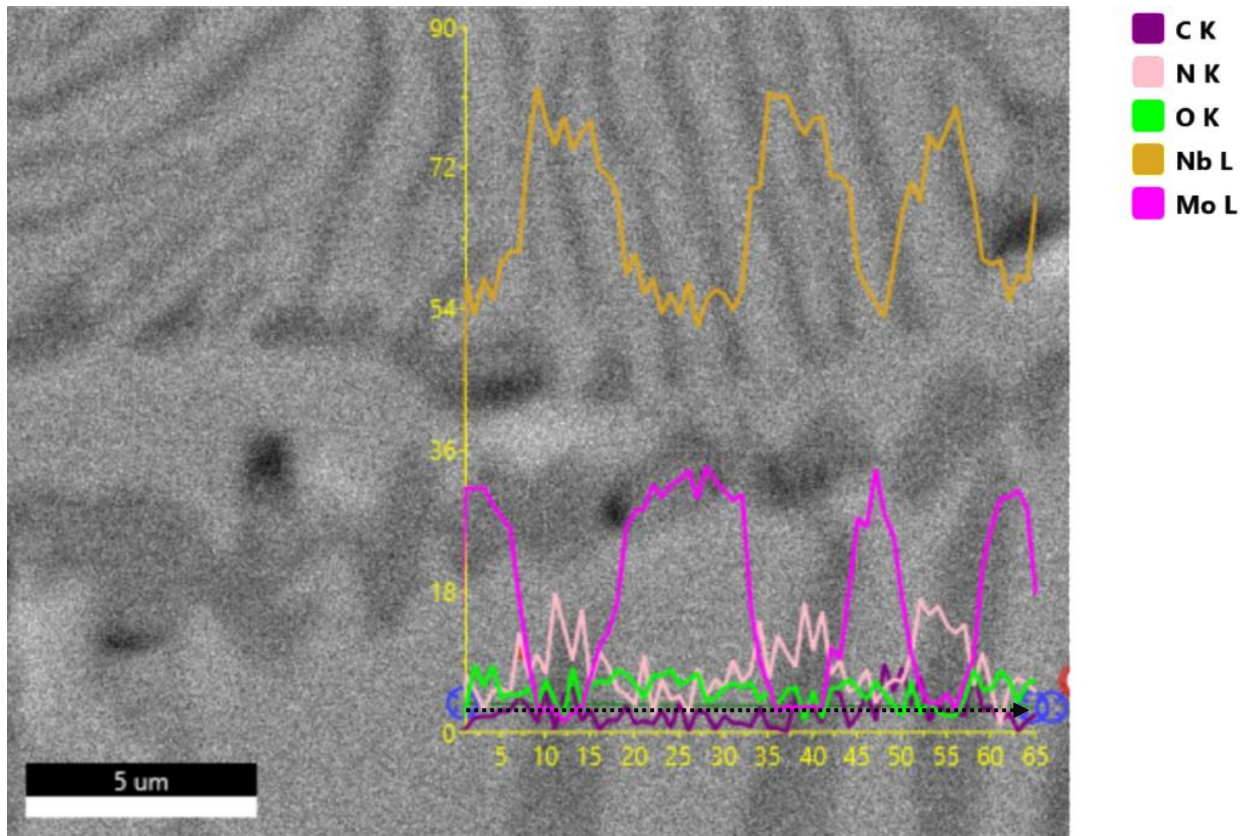
Figure 43.23: EDS line scan of Nb30Mo heat treated using the hot press at Mines in a flowing UHP Ar environment at 1700 ˚C for 68 h, where the black dashed line indicates where the line scan was performed.
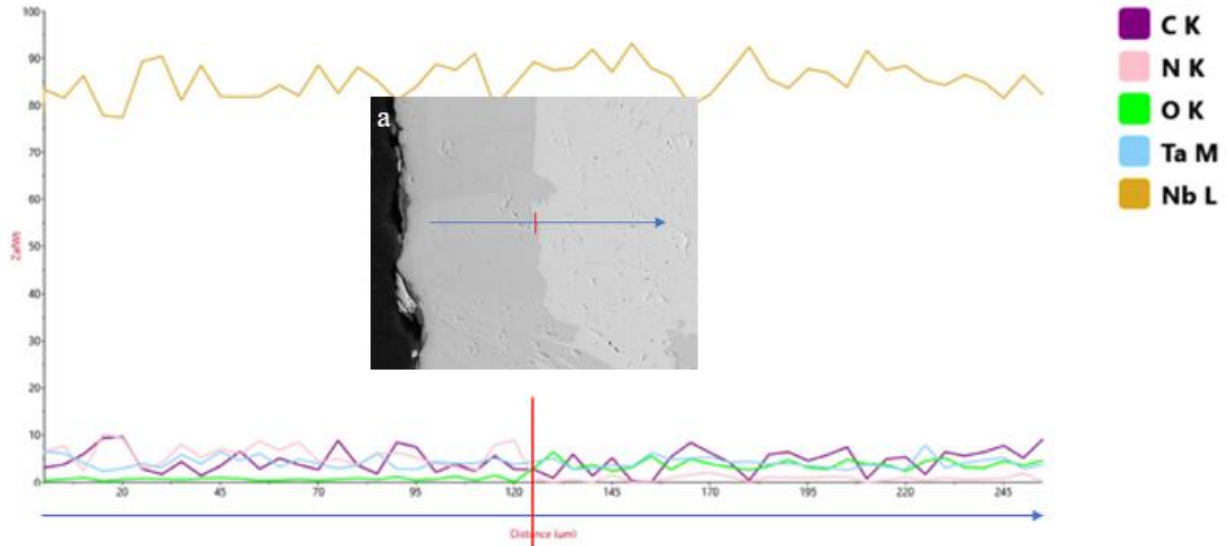
Figure 43.24: EDS line scan of Nb7.5Ta heat treated using the hot press at Mines in a flowing UHP Ar environment at 1700 ˚C for 68 h, where the blue line in image (a) indicates where the line scan was performed.
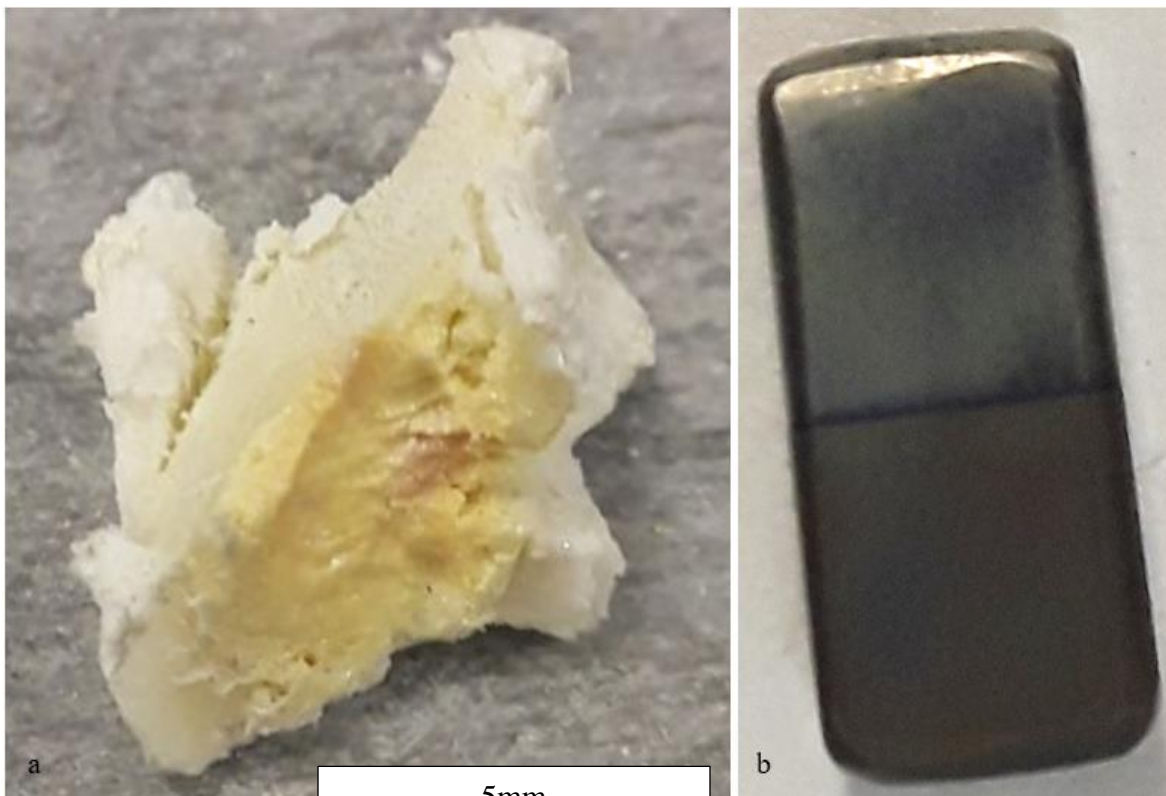
Figure 43.25: Mo-Ta diffusion co[...] the nesting doll diffusion chamber technique, where (a) was heat treated in a flowing Ar environment at 1500 ˚C for 72 h (second trial) and (b) was heat treated in air at 1500 ˚C for 24 h (first trial).